molecules

MDPI

Article

Discovery, Characterization, and Biosynthesis of Quinazolinone-Containing Desferrioxamines from Soil-Derived *Streptomyces platensis* CGMCC 4.1873

Lele Liu [1,2,†], Wenyu Zhang [2,†], Zhijun Tang [2,3,*] and Wen Liu [1,2,3,4,*]

[1] Department of Chemistry, University of Science and Technology of China, 96 Jinzhai Road, Hefei 230026, China; liulele@mail.ustc.edu.cn
[2] State Key Laboratory of Chemical Biology, Shanghai Institute of Organic Chemistry, University of Chinese Academy of Sciences, 345 Lingling Road, Shanghai 200032, China; z13966381141@163.com
[3] State Key Laboratory of Microbial Metabolism, School of Life Science & Biotechnology, Shanghai Jiao Tong University, Shanghai 200240, China
[4] Zhangjiang Institute for Advanced Study, Shanghai Jiao Tong University, Shanghai 201210, China
* Correspondence: tangzhijun1990@sjtu.edu.cn (Z.T.); wliu@sioc.ac.cn (W.L.); Tel.: +86-21-54925111 (W.L.); Fax: +86-21-64166128 (W.L.)
† These authors contributed equally to this work.

Abstract

Desferrioxamines are biologically important hydroxamate siderophores that facilitate microbial iron acquisition and have found therapeutic applications as iron chelators. Despite their biological and biomedical significance, desferrioxamines remain structurally underexplored, leaving considerable scope for the discovery of new architectures with expanded chemical and functional diversity. Here, we report the discovery and characterization of five desferrioxamines (**1**–**5**) from the soil-derived strain *Streptomyces platensis* CGMCC 4.1873, including four previously undescribed congeners (**2**–**5**) featuring unprecedented quinazolinone-containing scaffolds. Bioinformatic analysis identified a non-ribosomal peptide synthetase-independent siderophore biosynthetic gene cluster, *sgd*, responsible for the production of compounds **1**–**5**, which was confirmed by targeted in-frame deletion of the hydroxamate-forming gene *sgdB*. On the basis of genomic and structural analysis, we propose a plausible biosynthetic pathway for these unusual desferrioxamine derivatives. This study expands the chemical and biosynthetic diversity of desferrioxamines and provides new molecular scaffolds for exploring the functional potential of siderophores.

Keywords: secondary metabolites; *Streptomyces*; desferrioxamines; quinazolinone; biosynthesis

Check for updates

Academic Editor: Andrei Mocan

Received: 29 September 2026
Revised: 4 November 2026
Accepted: 5 November 2026
Published: 25 November 2026

Copyright: © 2026 by the authors. Licensee MDPI, Basel, Switzerland. This article is an open access article distributed under the terms and conditions of the Creative Commons Attribution (CC BY) license.

1. Introduction

Siderophores are low-molecular-weight iron-chelating metabolites produced by bacteria, fungi, and graminaceous plants that play central roles in iron acquisition and adaptation to iron-limited environments [1]. By forming highly stable complexes with ferric iron and delivering it through dedicated uptake systems comprising various membrane-associated receptors, siderophores enable microorganisms and plants to access an otherwise poorly bioavailable nutrient [2,3]. Beyond iron acquisition, siderophores also contribute to microbial competition [4], host–microbe interactions [5], and ecological fitness [6], while their strong and selective metal-binding properties have also stimulated applications in medicine and biotechnology [7]. More than 500 siderophores have been identified, encompassing diverse metal-chelating motifs, including hydroxamates, catecholates, and carboxylates,

together with a wide range of amino acid, fatty acid, and heterocyclic building blocks [8]. This structural diversity enables siderophores to adapt their physicochemical properties and biological functions to distinct ecological and physiological contexts.

The remarkable structural diversity of siderophores is enabled by versatile biosynthetic machineries, including polyketide synthases (PKSs), non-ribosomal peptide synthetases (NRPSs) and NRPS-independent siderophore (NIS) pathways [9–12]. PKSs and NRPSs employ modular assembly-line mechanisms to incorporate and modify activated acetate and amino acid precursors, thereby generating structurally diverse polyketide and peptide scaffolds [13,14]. In contrast, NIS pathways rely on discrete enzyme systems to assemble defined diamine and dicarboxylic acid building blocks, typically through iterative ATP-dependent amide-forming reactions [15]. Further structural diversification can be achieved through tailoring reactions, including acylation, hydroxylation, cyclization, and glycosylation, providing extensive opportunities for siderophore diversification.

Desferrioxamines are a prominent family of hydroxamate siderophores produced by diverse *Streptomyces* species and are distinguished by broad biological and biomedical relevance. The prototypical member of this family, desferrioxamine B, is clinically used as the iron-chelating drug, Desferal, for the treatment of iron overload [16]. Beyond their therapeutic iron chelation, desferrioxamines have been explored for metal-ion imaging and sensing, remediation of metal dyshomeostasis, and siderophore-mediated drug delivery [17–19]. Structurally, desferrioxamines consist of oligomeric *N*-hydroxy-*N*-succinylcadaverine units, with variations in number of repetitions, terminal groups, and cyclization giving rise to linear and cyclic congeners [20]. Their biosynthesis is primarily mediated by NIS pathways, in which ATP-dependent siderophore synthase assembles the hydroxamate-containing building blocks into the characteristic desferrioxamine scaffold [21]. Despite the biological and biomedical importance of this family, its structural diversity remains comparatively limited, particularly with respect to the incorporation of noncanonical heterocyclic architectures. Expanding the structural space of desferrioxamine could therefore provide new molecular scaffolds while revealing unexplored strategies for siderophore biosynthesis.

Here, we report the discovery and characterization of five desferrioxamines (**1**–**5**) (Figure 1) from the soil-derived strain *Streptomyces platensis* CGMCC 4.1873. Structural elucidation by HRMS, NMR spectroscopy, and X-ray crystallography uncovered that four of these metabolites (**2**–**5**) contain unprecedented quinazolinone-containing moieties. Bioinformatic analysis uncovered a dedicated NRPS-independent siderophore biosynthetic gene cluster, *sgd*, and gene deletion of the key hydroxamate-forming gene *sgdB* abolished the production of compounds **1**–**5**, establishing the involvement of this gene cluster in their biosynthesis. Integrating genomic and chemical data, we propose a biosynthetic route that accounts for the formation of these unusual quinazolinone-containing siderophores, providing insights into the biosynthetic diversification of the desferrioxamine family.

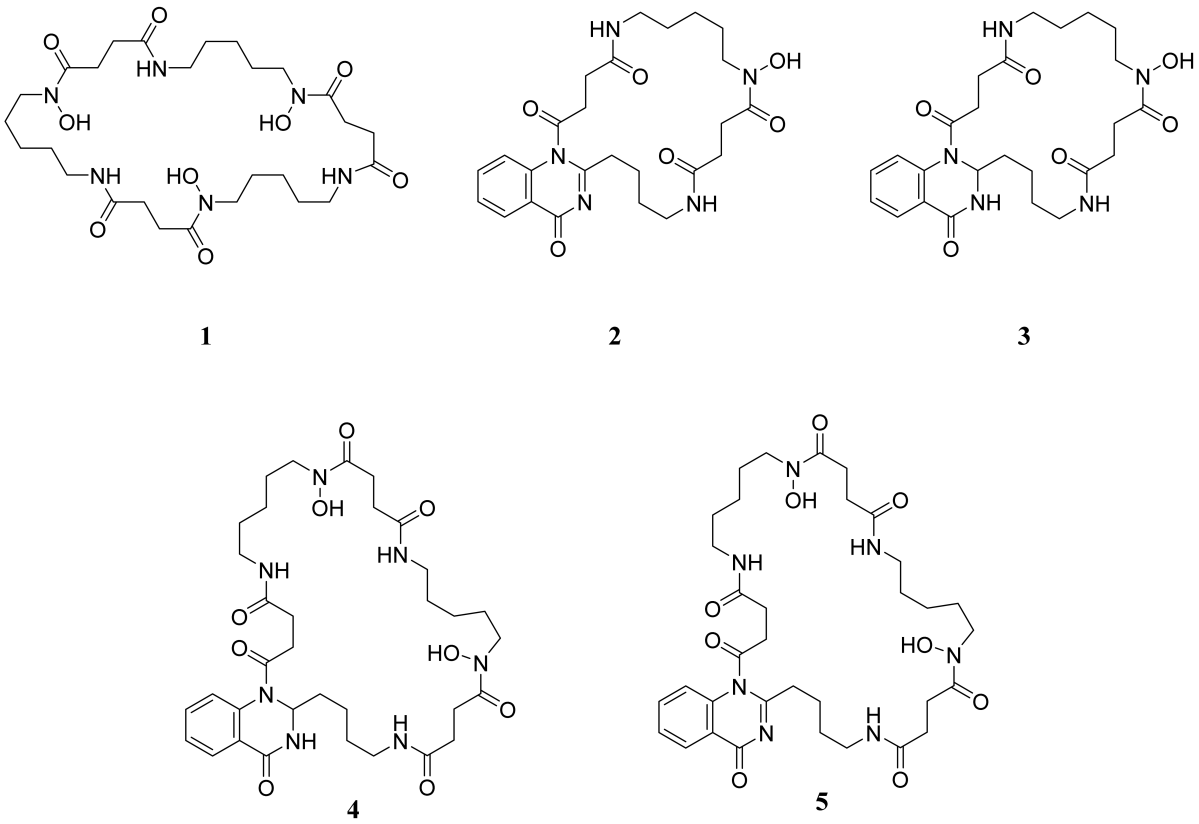


Figure 1. Chemical structures of desferrioxamine E (**1**) and desferrioxamines I–L (**2**–**5**).

2. Results and Discussion

*2.1. Discovery of Desferrioxamine E (**1**) and Desferrioxamines I–L (**2**–**5**)*

S. platensis CGMCC 4.1873 was cultivated in liquid GYM medium for 7 days. The cell pellets and culture supernatants were extracted separately with methanol and ethyl acetate, respectively. The resulting extracts were concentrated to dryness under reduced pressure. High-performance liquid chromatography-mass spectrometry (HPLC-MS) analysis identified fractions containing the desired metabolites, which were subsequently purified by semi-preparative HPLC to afford compounds **1**–**5** (Figure 1). The detailed separation procedure is shown in Figure S1. The structures of compounds **1**–**5** were elucidated by a combination of HRMS, NMR spectroscopy, spectral data and X-ray crystallography (Figures S2–S43). The structure of compound **1** was unambiguously determined by X-ray crystallographic analysis (CCDC: 2582741), while compounds **2**–**5** were established based on HRMS and comprehensive 2D NMR spectroscopic analyses.

Desferrioxamine E (**1**) was obtained as white needle-shaped crystals during purification by ODS (octadecylsilyl) reversed-phase column chromatography. Ultraviolet–visible (UV) (MeOH) λ_{max} 191 nm (Figure S4); IR (ATR) ν_{max}/cm^{-1} 2952, 1657, 1621, 1554, 1463, 1385, 1366, 1252, 1227, 1155, 1112. Its structure was unambiguously established by single-crystal X-ray diffraction analysis (Figure S3) and further supported by HRMS data (Figure S2), which showed an $[M + H]^+$ ion at *m*/*z* 601.3570 (calcd. for 601.3556, error 2.33 ppm), confirming compound **1** as the known desferrioxamine E [22].

Desferrioxamine I (**2**) was obtained as yellow oil. UV (MeOH) λ_{max} 202 nm (Figure S6); IR (MeOH) ν_{max}/cm^{-1} 3021, 2932, 1770, 1693, 1609, 1568, 1468, 1440, 1404, 1339, 1250, 1163, 820, 777, 732, 662. HRESIMS *m*/*z* 500.2507 $[M + H]^+$ (calcd for $C_{25}H_{34}N_5O_6$, 500.2504, error 0.60 ppm) corresponding to 12 degrees of unsaturation (Figure S5). Analysis of the ^1H, ^{13}C, and distortionless enhancement by polarization transfer (DEPT) spectra (Figures S7–S9)

revealed the presence of five amide carbonyl groups [δ_C 180.18, 180.18, 174.6, 175.1], and an *ortho*-disubstituted benzene ring moiety [δ_H 8.18 (1H, d), 7.50 (1H, t), 7.81 (1H, t) and 7.65 (1H, d); δ_C 121.0, 127.1, 127.6, 135.9, 127.4 and 150.1], one quaternary carbon, thirteen methylenes (Table 1). The δ_C values of C-9′ (δ_C 160.05) and C-10 (δ_C 164.20) were assigned on the basis of HMBC correlations (Figure 2 and Table 1), as these signals were not clearly resolved in the ^{13}C/DEPT spectra (Figures S8 and S9). Extensive signal overlap was observed in the NMR spectra, suggesting the presence of structurally similar repeating units. Detailed analysis of the 1D and 2D NMR spectroscopic data (Figures S7–S14) allowed for the unambiguous assignment of all proton signals to their corresponding carbon resonances.

Table 1. The ^{1}H, ^{13}C NMR data of compounds **2** and **4** in methanol-d_4.

No.	**2 (Methanol-d_4)**		No.	**4 (Methanol-d_4)**	
	δ_H (J in Hz) (600 MHz)	**δ_C (150 MHz)**		**δ_H (J in Hz) (600 MHz)**	**δ_C (150 MHz)**
1		180.18 [b]	1		180.05 [b]
2	2.67, s [a]	29.09 [b]	2	2.67, s [a]	29.09 [b]
3	2.67, s [a]	29.09 [b]	3	2.67, s [a]	29.09 [b]
4		180.18 [b]	4		180.05 [b]
5	3.44, t (7.1)	39.4	5	3.46, t (7.1)	39.2
6	1.55, m	28.1	6 6′	1.56, m	28.2
7	1.26, m	24.8	7 7′	1.27, m	24.8
8	1.61, m	27.2	8 8′	1.62, m	27.3
9	3.56, t (6.8)	49.0	9 9′	3.58, m	48.8
1′		174.6	1′ 1″		174.4
2′	2.46, t (7.1)	31.5	2′ 2″	2.45, m	31.4
3′	2.77, t (7.1)	28.8	3′ 3″	2.77, m	28.8
			4′		174.9
			5′	3.14, t (6.8)	40.3
4′		175.2	4″		175.0
5′	3.25, t (6.6)	39.7	5″	3.21, t (5.8)	39.9
6′	1.58, m	29.1	6″	1.52, m	21.9
7′	1.84, m	26.0	7″	1.53, m	30.1
8′	2.71, m	35.6	8″	1.75, m	35.7
9′		160.0 [c]	9″	4.79, t (4.9)	66.2
10		164.2 [c]	10		167.7
11		121.0 [c]	11		115.9
12	8.18, d (8.2)	127.1	12	7.68, d (7.3)	128.7
13	7.50, dd (8.2, 7.0)	127.6	13	6.73, m	118.9
14	7.81, dd (8.2, 7.0)	135.9	14	7.27, t (7.3)	135.0
15	7.65, d (8.2)	127.4	15	6.74, m	115.8
16		150.1 [c]	16		150.1

[a] overlapped signals in ^{1}H NMR, [b] overlapped signals in ^{13}C NMR, [c] HMBC correlations are from proton(s) to stated carbons.

Analysis of the ^{1}H–^{1}H homonuclear correlation spectroscopy (COSY) spectrum revealed three major spin systems. The first comprises two repeating motifs, H-5 to H-8 and H-5′ to H-8′, while the second consists of two repeating motifs, H-2 to H-3 and H-2′ to H-3′, the third consists of a single spin system spanning H-12 to H-15. In the heteronuclear multiple-bond correlation (HMBC) spectrum, key correlations from H-3 to C-1, H-2 to C-4, H-5 to C-4, H-9 to C-1′, H-3′ to C-1′, H-2′ to C-4′, H-5′ to C-4′, H-8′ to C-9′ and H-12 to C-10 were observed, allowing the establishment of the planar structure of desferrioxamine

I (**2**) (Figure 2). To the best of our knowledge, this is the first reported occurrence of a 4(*1H*)-quinazolinone scaffold in a desferrioxamine-type molecule.

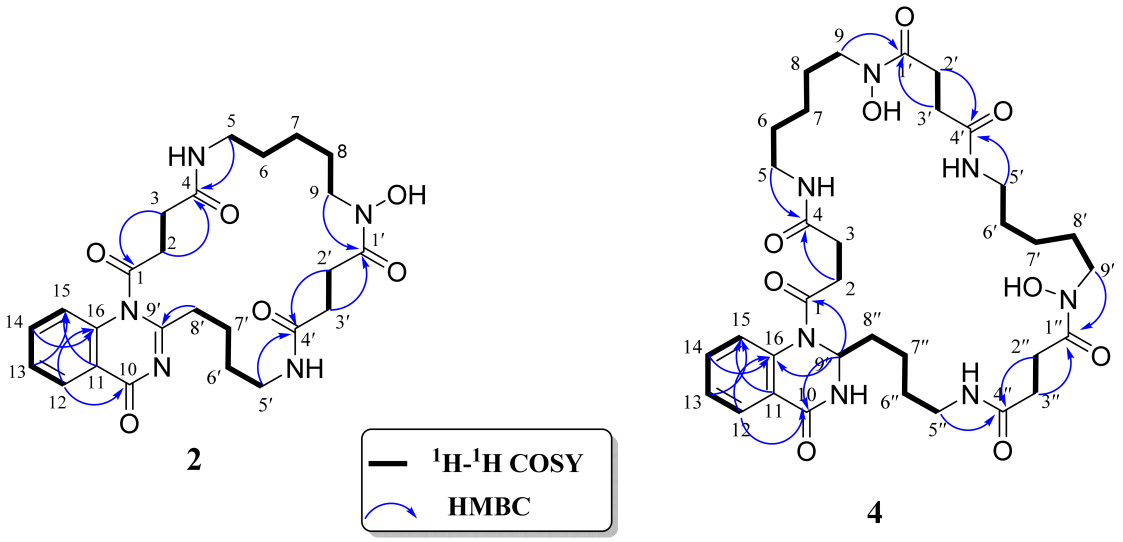


Figure 2. Key relevant NMR correlations used to elucidate the structure of compounds **2** and **4**.

Desferrioxamine J (**3**) was obtained as yellow oil. Its molecular formula was determined to be $C_{25}H_{35}N_5O_6$ based on HRMS (Figure S15), which showed an $[M + H]^+$ ion at *m/z* 502.2670 (calcd. for 502.2660, error 1.99 ppm), indicating 11 degrees of unsaturation and a molecular mass 2 Da higher than that of desferrioxamine I. During isolation and characterization, desferrioxamine J proved highly susceptible to conversion into desferrioxamine I upon heating, which resulted in poor-quality NMR data (Figures S16–S22). Nevertheless, comparison of the HRMS data and tandem mass spectrometric (MS/MS) fragmentation patterns of desferrioxamines I and J allowed us to propose that desferrioxamine J contains a 2,3-dihydroquinazolin-4(*1H*)-one moiety (Figure S44). This proposed structural assignment is also consistent with the well-documented propensity of quinazoline derivatives to undergo oxidation to the corresponding quinazolinones [23,24]. Further comparison of the NMR data of desferrioxamines I and J provided additional support for the proposed structure of desferrioxamine J (Table S1). Key relevant NMR correlations used to elucidate the structure of compound **3** are shown in Figure S23.

Given the oxidative instability of desferrioxamine J, desferrioxamine K (**4**) was purified under low-temperature conditions to minimize oxidative degradation. The semi-preparative HPLC fraction containing desferrioxamine K was immediately lyophilized and directly subjected to NMR analysis, enabling its structural characterization. Desferrioxamine K was obtained as yellow powder. Its molecular formula was determined to be $C_{34}H_{51}N_7O_9$ based on HRMS (Figure S24), which showed an $[M + H]^+$ ion at *m/z* 702.3830 (calcd. for 702.3821, error 1.28 ppm), corresponding to 13 degrees of unsaturation. The MS/MS fragmentation pattern of desferrioxamine K closely resembled that of desferrioxamine J, suggesting that they share a similar structural framework (Figure S44). This assignment was further supported by analysis of the ^{1}H, ^{13}C, and DEPT NMR spectra (Figures S25–S27). Although extensive signal overlap was observed in the NMR spectra, detailed analysis of the 2D NMR data enabled the complete assignment of the corresponding proton and carbon signals (Figures S28–S32). Compared with desferrioxamine I, desferrioxamine K displayed two additional repeating spin systems in the ^{1}H–^{1}H COSY spectrum, corresponding to H-2″ to H-3″ and H-5″ to H-9″ (Figure 2 and Table 1). Key HMBC correlations, including H-9″ to C-1, H-2 to C-4, H-5 to C-4, H-9 to C-1′, H-3′ to C-1′, H-2′ to C-4′, H-5′ to C-4′, H-9′ to C-1″, H-3″ to C-1″, H-2″ to C-4″, H-5″ to C-4″, H-9″ to C-10, H-9″ to C-16 and H-12 to

C-10 further established the planar structure of desferrioxamine K (Figure 2). This finding further corroborated the proposed structure of desferrioxamine J.

Desferrioxamine L (**5**) was obtained as yellow powder. UV (MeOH) λ_{max} 199 nm (Figure S34); IR (MeOH) ν_{max}/cm^{-1} 3302, 2932, 1771, 1694, 1601, 1558, 1468, 1405, 1373, 1251, 1167, 1002, 877, 821, 776, 734, 699, 663, 588, 496. HRESIMS *m/z* 700.3677 [M + H]$^+$ (calcd for $C_{34}H_{50}N_7O_9$, 700.3665, error 1.71 ppm), corresponding to 14 degrees of unsaturation (Figure S33) and it exhibits that desferrioxamine L has a molecular mass 2 Da lower than that of desferrioxamine K. Although high-quality NMR data could not be obtained to unambiguously define its structure, the MS/MS fragmentation pattern of desferrioxamine L closely resembled that of desferrioxamine K (Figure S44), suggesting that these two compounds share a highly similar structural framework. Further comparison of the NMR data of desferrioxamines L and K supports the assignment of compound **5** as desferrioxamine L, featuring a quinazolinone derived from oxidation of the corresponding quinazoline moiety (Figures S37–S43).

Following structural elucidation, compounds **1**, **2**, and **5** were selected for evaluation of their potential iron-chelating activity using the chrome azurol S (CAS) assay due to their stability and sufficient availability. These compounds induced only slight color changes relative to the negative control (methanol), whereas EDTA produced a pronounced color change, indicating weak iron-chelating activity under the tested conditions (Figure S48).

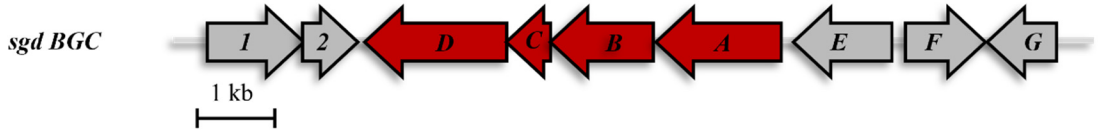
2.2. Biosynthetic Gene Cluster Identification and Proposed Biosynthetic Pathway

Following the structural elucidation of compounds **1**–**5**, we next sought to elucidate their biosynthetic origin, with particular interest in the formation of the unusual quinazolinone scaffold. Inspired by the established desferrioxamine biosynthetic pathway, we used the FAD-dependent amine monooxygenase DesB [25], which is essential for hydroxamate formation, as a query to search the genome of *S. platensis* CGMCC 4.1873. This analysis identified a candidate biosynthetic gene cluster, designated the *sgd* BGC, spanning approximately 12 kb and comprising nine open reading frames (ORFs) (Table 2), including *sgdB*, a homolog of *desB* (Figure S45), and *sgdD*, which encodes a putative ATP-dependent siderophore synthase characteristic of canonical NRPS-independent siderophore biosynthetic pathways. The *sgd* BGC shares substantial sequence similarity with the canonical desferrioxamine *des* BGC (Figure S45) [26], supporting its involvement in the biosynthesis of compounds **1**–**5**.

To establish a genetic link between the *sgd* BGC and compounds **1**–**5**, we generated an in-frame deletion of *sgdB* using a homologous recombination-based double-crossover strategy. The resulting Δ*sgdB* mutant strain was verified by PCR and DNA sequencing (Figure S46) and cultured alongside the wild-type strain under identical conditions. Strikingly, HPLC-MS analysis of the culture supernatants revealed that production of all five compounds was abolished in the Δ*sgdB* mutant strain (Figure 3). These results demonstrate that *sgdB* is essential for the production of compounds **1**–**5** and provide genetic evidence supporting the assignment of the *sgd* BGC as their biosynthetic locus.

Based on the predicted functions of the encoded proteins and comparison with the canonical desferrioxamine pathway, we propose a biosynthetic pathway for compounds **1**–**5** (Figure 4). L-Lysine is first converted to cadaverine by a PLP-dependent decarboxylase SgdA, followed by *N*-hydroxylation by the FAD-dependent monooxygenase SgdB, to afford *N*-hydroxycadaverine. Subsequent *N*-succinylation is proposed to yield *N*-hydroxy-*N*-succinylcadaverine, the monomeric building block of desferrioxamines. ATP-dependent oligomerization by the siderophore synthetase SgdD would then generate the corresponding dimeric and trimeric intermediates. Similar to the canonical desferrioxamine pathway, the DesD homolog SgdD catalyzes subsequent cyclization to furnish desferrioxamine E (**1**).

Table 2. Organization and proposed functions of the ORFs in the *sgd* BGC from *S. platensis* CGMCC 4.1873.



Gene	Size [a]	Proposed Function	Protein Homolog (Accession No.)	I/C [b]
1	412	hypothetical protein	WP_405845525.1	91/100
2	236	TPR family protein	QEV51766.1	97/100
D	605	ATP-dependent siderophore synthetase	WP_386447235.1	92/100
C	189	*N*-acetyltransferase	WP_406217098.1	94/100
B	439	lysine-6-monooxygenase	WP_311625711.1	92/100
A	535	PLP dependent decarboxylase	WP_190141134.1	100/100
E	421	putative transcriptional regulator	WP_453262847.1	91/100
F	341	hydrolase	BAV57076.1	35/74
G	296	siderophore interacting protein	QKS42876.1	62/97

[a] amino acids (aa), [b] identity/coverage.

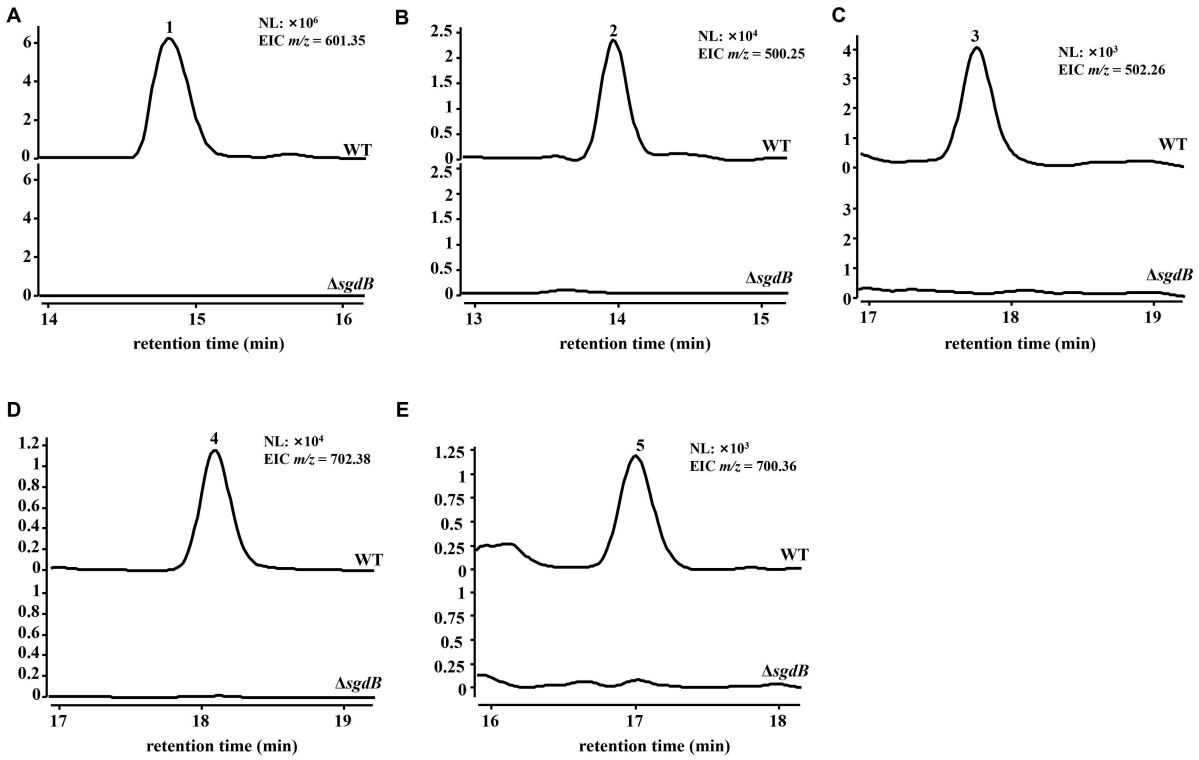


Figure 3. LC–MS analysis of metabolites produced by the wild-type (WT) and Δ*sgdB* strains. For extracted ion chromatograms (EICs), the ESI *m*/z values of $[M + H]^+$ modes for compounds **1**–**5** (**A**–**E**) are 601.35, 500.25, 502.26, 702.38, 700.36, respectively. Compounds **1**–**5** were not detected in the Δ*sgdB* mutant.

In contrast, the biosynthesis of compounds **2**–**5** is proposed to involve the incorporation of anthranilic acid into dimeric or trimeric desferrioxamine precursors. Anthranilic acid can be derived from chorismate through the action of anthranilate synthase, for which a putative encoding gene was identified elsewhere in the genome of *S. platensis* CGMCC 4.1873, rather than within the *sgd* BGC. Previous studies by Zou and co-workers on chrysogine biosynthesis demonstrated that the 4(*3H*)-quinazolinone scaffold is assembled through NRPS-mediated anthranilate incorporation, followed by enzymatic tailoring and sponta-

neous cyclization [27]. However, no NRPS with a similar function was identified within the *sgd* BGC, suggesting that anthranilic acid incorporation may be mediated by alternative amide-bond-forming enzymes [28,29]. Two possible routes can be envisioned, differing in the initial condensation step and the sequence of macrocyclization and heterocycle formation. Anthranilic acid could first be incorporated through condensation of its carboxyl group with the terminal amino group of the desferrioxamine precursor or, alternatively, through coupling of its amino group with the terminal carboxyl group of the precursor. Subsequent formation of the second amide bond could complete macrocyclization, affording intermediates **Int-1** or **Int-2**, which may undergo dehydration and intramolecular cyclization to generate the dihydroquinazolinone moiety (Figure 4). Alternatively, formation of the dihydroquinazolinone ring may precede macrocyclization, followed by intramolecular amide bond formation to afford compounds **3** and **4** (Figure S47). Subsequent oxidation could then yield the corresponding quinazolinone derivatives **2** and **5**, respectively. Nevertheless, the enzymes involved and the precise sequence of these transformations remain to be experimentally established.

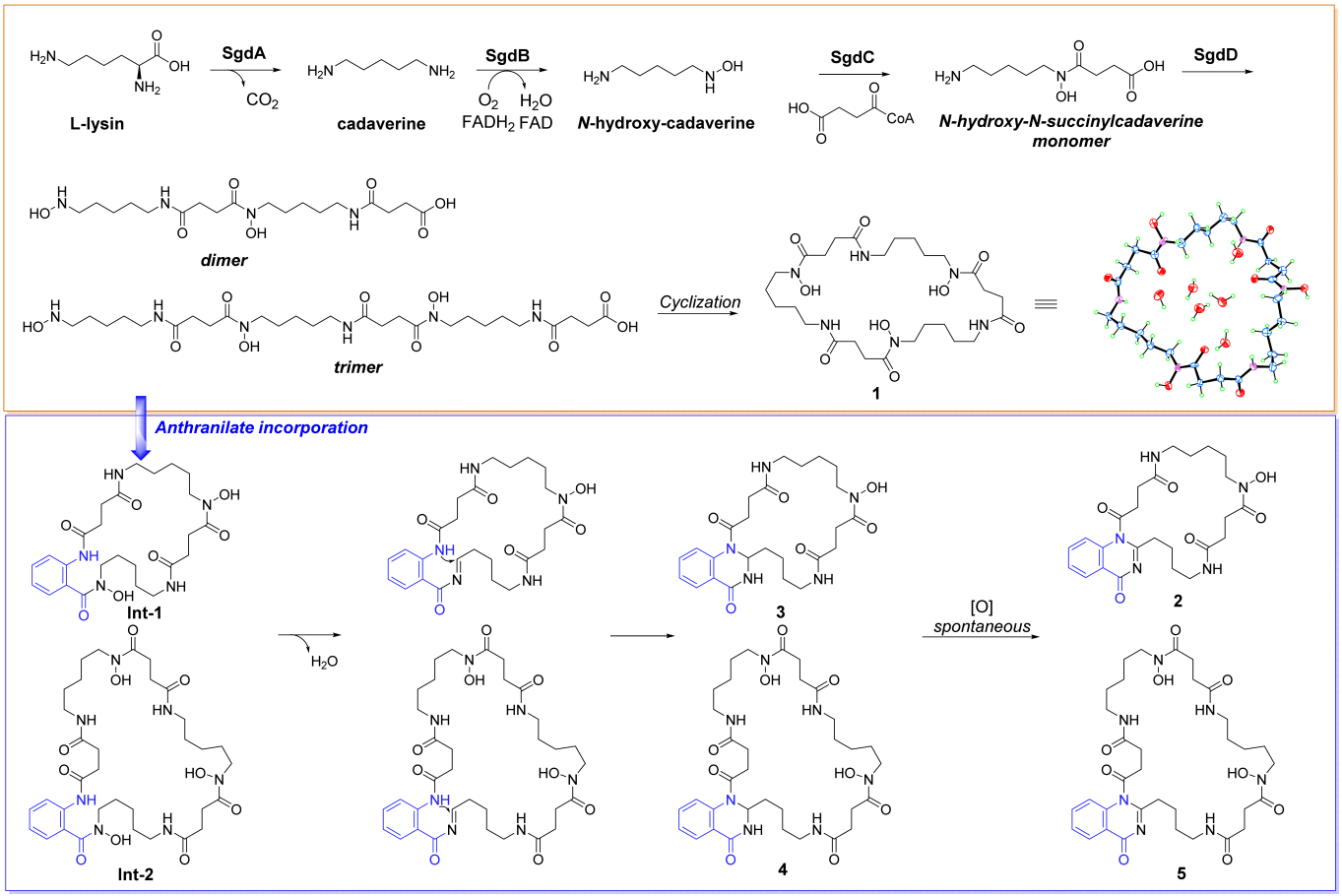


Figure 4. Proposed biosynthetic pathways for desferrioxamine E (**1**) and desferrioxamines I–L (**2**–**5**). The established pathway to **1** is shown in orange, whereas the proposed pathway to **2**–**5**, involving anthranilate incorporation and sequential amide-bond formation, is shown in blue.

3. Materials and Methods

3.1. Materials, Bacterial Strains, and Plasmids

Biochemicals and media were purchased from Sinopharm Chemical Reagent, Oxoid Ltd. (Shanghai, China), or Sigma-Aldrich (St. Louis, MO, USA) unless otherwise stated. Restriction endonucleases were purchased from Thermo Fisher Scientific (Shanghai, China)

and New England Biolabs (Beijing, China). Chemical reagents were purchased from standard commercial sources. The bacterial strains, plasmids, and primers used in this study are summarized in Tables S2, S3, and S4, respectively.

3.2. DNA Isolation, Manipulation, and Sequencing

DNA isolation and manipulation in *E. coli* or *Streptomyces* strains were carried out according to standard methods. PCR amplifications were carried out on an Applied Biosystems Veriti Thermal Cycler (Thermo Fisher Scientific Co., Ltd., Shanghai, China) using either Taq DNA polymerase (Vazyme Biotech Co., Ltd., Nanjing, Jiangsu, China) for routine genotype verification or PrimeSTAR HS DNA polymerase (Takara Biotechnology (Dalian) Co., Ltd., Dalian, Liaoning, China) for high-fidelity amplification. Primer synthesis and DNA sequencing was performed at Shanghai Biosune Biological Technology (Shanghai, China).

3.3. Constructs for Gene Inactivation in S. platensis CGMCC 4.1873

The genomic DNA of *S. platensis* CGMCC 4.1873 wild-type was used as the template. For inactivation of *sgdB*, a 1.92-kb fragment was obtained by PCR amplification using the primers SgdB-LF/SgdB-LR, while a 2.02-kb fragment was obtained by PCR amplification using the primers SgdB-RF/SgdB-RR. These two DNA fragments were co-ligated in pYH7 to yield the recombinant plasmid pΔ*sgdB*, in which an 885-bp internal sequence region of *sgdB* was deleted in-frame.

The introduction of the above recombinant plasmid into *S. platensis* CGMCC 4.1873 wild-type was carried out by *E. coli* ET12567-*Streptomyces* conjugation [30]. A colony of the *E. coli* ET12567 strain that harbors the recombinant plasmid was inoculated in 25 mL of Luria–Bertani (LB) medium (yeast extract 0.5%, tryptone 1% and NaCl 1%, pH 7.2) containing 50 μg of kanamycin/mL, 25 μg of chloramphenicol/mL and 50 μg of apramycin/mL, followed by incubation at 37 °C and 220 rpm until the cell density reached 0.4-0.6 at OD_{600}. The cells were washed twice with LB and resuspended in 1 mL of LB to provide the donor *E. coli* culture. The *S. platensis* CGMCC 4.1873 spores grown on solid MS medium (D-Mannitol 2%, Soya flour 2% and Agar 2%, pH 7.2) were resuspended in 1 mL of LB medium and washed twice with 1 mL LB medium. The recipient *S. platensis* CGMCC 4.1873 culture was generated by inoculating 1 mL of LB medium with *S. platensis* CGMCC 4.1873 spores for heat shock treatment 10 min at 50 °C, followed by further incubation for 3 h at 37 °C. The donor and recipient cultures were mixed with a ratio of 1:1 and 1:2.

3.4. Production, Purification and Characterization of Desferrioxamines (Compounds **1**–**5***)*

S. platensis CGMCC 4.1873 strains were grown on solid MS medium at 30 °C for 4 d. The spores of each strain were inoculated into 100 mL liquid TSB medium (3% tryptic soy broth) in a 500 mL flask, followed by incubation at 30 °C and 220 rpm for 48 h. The culture of each strain was inoculated into 150 mL liquid GYM (glucose 0.4%, yeast extract 0.4%, malt extract 1%, N-Z amine 0.1%, NaCl 0.2%, pH 7.2) medium in a 500 mL flask, followed by incubation in the dark at 30 °C and 220 rpm for 7 d. After centrifugation, the cell pellets and culture supernatants were extracted separately with methanol and ethyl acetate, respectively. Combined extracts were concentrated by vacuum and purified through chromatography on silica gel and an ODS column. The detailed procedures were described in Figure S1 of the Supplementary Information.

3.5. Chemical Analysis

HPLC analysis was carried out on an Agilent 1260 HPLC system (Agilent Technologies, Santa Clara, CA, USA) equipped with a DAD detector (Agilent Technologies). Semi-preparative HPLC was performed on an Agilent 1100 system equipped with a DAD detector.

HR-MS analysis for small molecules was carried out on an Agilent 6230B Accurate Mass TOF LC-MS. Analyses by HPLC-associated ESI HR-MS/MS were performed on a Q Exactive Plus Mass Spectrometer (Thermo Fisher Scientific, Waltham, MA, USA). Related data were processed using Thermo Xcalibur software (4.3 + NIST Libraries). NMR data were recorded on a Bruker Avance Neo 500 NMR spectrometer (Bruker Corporation, Billerica, MA, USA).

3.6. Genome Sequencing and BGCs Mining

The genome of *S. platensis* CGMCC 4.1873 was sequenced by Shanghai Personalbio Technology Co., Ltd. (Shanghai, China) with a combination of next-generation sequencing using Illumina MiSeq and long-read sequencing using PacBio RS platforms. Then, bioinformatics analysis succeeded in assembling the whole genome from the generated sequence data. AntiSMASH 8.0 [31] and BLAST+2.17.0 were used for the analysis of the potential BGCs of *S. platensis* CGMCC 4.1873, especially the *sgd* BGC, followed by manual verification.

3.7. CAS Assay Preparation

The iron-chelating activity of compounds **1**, **2**, and **5** was evaluated using the chrome azurol S (CAS) assay. The CAS reagent was prepared according to a previously reported procedure [32]. The compounds were dissolved in methanol at a concentration of 200 μM. EDTA (200 μM) and methanol served as the positive and negative controls, respectively. Each sample or control solution (100 μL) was mixed with CAS reagent (100 μL).

4. Conclusions

In summary, we have discovered and characterized five desferrioxamines (**1**–**5**) from the soil-derived *S. platensis* CGMCC 4.1873, including four previously undescribed congeners featuring unprecedented quinazolinone-containing scaffolds. Genetic analysis identified that the *sgd* biosynthetic gene cluster is responsible for their production, as supported by the complete loss of **1**–**5** upon deletion of the essential hydroxamate-forming gene *sgdB*. Integrating structural, genomic, and biosynthetic analyses, we propose a biosynthetic pathway in which anthranilic acid is incorporated into desferrioxamine assembly to generate the unusual quinazolinone-containing structures. This study expands the structural and biosynthetic diversity of the desferrioxamine family and highlights the potential of NIS pathways to generate noncanonical siderophore architectures.

Supplementary Materials: The following supporting information can be downloaded at: https://www.mdpi.com/article/10.3390/molecules31234289/s1, NMR data, structure elucidation of all isolated compounds, and crystal structure information are included.

Author Contributions: L.L. and W.Z. contributed equally to this work. Z.T. and W.L. conceived and designed the research. L.L. and W.Z. conducted all structure isolation, characterization, and biochemical experiments. L.L., W.Z., Z.T., and W.L. analyzed data and discussed results. L.L., W.Z., Z.T., and W.L. prepared the manuscript. All authors have read and agreed to the published version of the manuscript.

Funding: This work is part of the Shanghai Municipal Science and Technology Major Project, and was supported in part by grants from the Shanghai Rising-Star Program (24QA2711500), and the Shanghai Commission of Science and Technology (24HC2820300).

Data Availability Statement: The original contributions presented in this study are included in the article/Supplementary Materials. Further inquiries can be directed to the corresponding authors.

Conflicts of Interest: The authors declare no conflicts of interest.

References

1. Hider, R.C.; Kong, X. Chemistry and biology of siderophores. *Nat. Prod. Rep.* **2010**, *27*, 637–657. [CrossRef] [PubMed]
2. Nader, S.; Pérard, J.; Carpentier, P.; Arnaud, L.; Crouzy, S.; Michaud-Soret, I. New insights into the tetrameric family of the Fur metalloregulators. *Biometals* **2019**, *32*, 501–519. [CrossRef] [PubMed]
3. Sheldon, J.R.; Heinrichs, D.E. Recent developments in understanding the iron acquisition strategies of gram positive pathogens. *FEMS Microbiol. Rev.* **2015**, *39*, 592–630. [CrossRef] [PubMed]
4. Kramer, J.; Özkaya, Ö.; Kümmerli, R. Bacterial siderophores in community and host interactions. *Nat. Rev. Microbiol.* **2020**, *18*, 152–163. [CrossRef] [PubMed]
5. Ellermann, M.; Arthur, J.C. Siderophore-mediated iron acquisition and modulation of host-bacterial interactions. *Free Radic. Biol. Med.* **2017**, *105*, 68–78. [CrossRef] [PubMed]
6. Codd, R.; Richardson-Sanchez, T.; Telfer, T.J.; Gotsbacher, M.P. Advances in the Chemical Biology of Desferrioxamine B. *ACS Chem. Biol.* **2017**, *13*, 11–25. [CrossRef] [PubMed]
7. Schalk, I.J. Bacterial siderophores: Diversity, uptake pathways and applications. *Nat. Rev. Microbiol.* **2025**, *23*, 24–40. [CrossRef] [PubMed]
8. Boukhalfa, H.; Crumbliss, A.L. Chemical aspects of siderophore mediated iron transport. *Biometals* **2002**, *15*, 325–339. [CrossRef] [PubMed]
9. Quadri, L.E.N.; Sello, J.; Keating, T.A.; Weinreb, P.H.; Walsh, C.T. Identification of a *Mycobacterium tuberculosis* gene cluster encoding the biosynthetic enzymes for assembly of the virulence-conferring siderophore mycobactin. *Chem. Biol.* **1998**, *5*, 631–645. [CrossRef] [PubMed]
10. Crosa Jorge, H.; Walsh Christopher, T. Genetics and Assembly Line Enzymology of Siderophore Biosynthesis in Bacteria. *Microbiol. Mol. Biol. Rev.* **2002**, *66*, 223–249. [CrossRef] [PubMed]
11. Keatinge-Clay, A.T. The Uncommon Enzymology of Cis-Acyltransferase Assembly Lines. *Chem. Rev.* **2017**, *117*, 5334–5366. [CrossRef] [PubMed]
12. Fischbach, M.A.; Walsh, C.T. Assembly-Line Enzymology for Polyketide and Nonribosomal Peptide Antibiotics: Logic, Machinery, and Mechanisms. *Chem. Rev.* **2006**, *106*, 3468–3496. [CrossRef] [PubMed]
13. Singh, M.; Chaudhary, S.; Sareen, D. Non-ribosomal peptide synthetases: Identifying the cryptic gene clusters and decoding the natural product. *J. Biosci.* **2017**, *42*, 175–187. [CrossRef] [PubMed]
14. Roche, B.; Mislin, G.L.A.; Schalk, I.J. Identification of the fatty acid coenzyme-A ligase FadD1 as an interacting partner of FptX in the *Pseudomonas aeruginosa* pyochelin pathway. *FEBS Lett.* **2021**, *595*, 370–378. [CrossRef] [PubMed]
15. Telfer, T.J.; Gotsbacher, M.P.; Soe, C.Z.; Codd, R. Mixing Up the Pieces of the Desferrioxamine B Jigsaw Defines the Biosynthetic Sequence Catalyzed by DesD. *ACS Chem. Biol.* **2016**, *11*, 1452–1462. [CrossRef] [PubMed]
16. Ribeiro, M.; Sousa, C.A.; Simões, M. Harnessing microbial iron chelators to develop innovative therapeutic agents. *J. Adv. Res.* **2022**, *39*, 89–101. [CrossRef] [PubMed]
17. Haas, K.L.; Franz, K.J. Application of Metal Coordination Chemistry To Explore and Manipulate Cell Biology. *Chem. Rev.* **2009**, *109*, 4921–4960. [CrossRef] [PubMed]
18. Petrik, M.; Zhai, C.; Haas, H.; Decristoforo, C. Siderophores for molecular imaging applications. *Clin. Transl. Imaging* **2017**, *5*, 15–27. [CrossRef] [PubMed]
19. Schalk, I.J. A Trojan-Horse Strategy Including a Bacterial Suicide Action for the Efficient Use of a Specific Gram-Positive Antibiotic on Gram-Negative Bacteria. *J. Med. Chem.* **2018**, *61*, 3842–3844. [CrossRef] [PubMed]
20. Wang, Z.-J.; Zhou, H.; Zhong, G.; Huo, L.; Tang, Y.-J.; Zhang, Y.; Bian, X. Genome Mining and Biosynthesis of Primary Amine-Acylated Desferrioxamines in a Marine Gliding Bacterium. *Org. Lett.* **2020**, *22*, 939–943. [CrossRef] [PubMed]
21. Yang, J.; Banas, V.S.; Rivera, G.S.M.; Wencewicz, T.A. Siderophore Synthetase DesD Catalyzes N-to-C Condensation in Desferrioxamine Biosynthesis. *ACS Chem. Biol.* **2023**, *18*, 1266–1270. [CrossRef] [PubMed]
22. Li, J.; Cheng, B.; Huang, J.; Liu, W. Study on Isolation, Identification and Bioactivity of Desferrioxamine E and Its Metal-Complexes from *Streptacidiphilus jiangxiensis*. *Chin. J. Org. Chem.* **2024**, *44*, 2377–2380. [CrossRef]
23. Asif, M. Chemical Characteristics, Synthetic Methods, and Biological Potential of Quinazoline and Quinazolinone Derivatives. *Int. J. Med. Chem.* **2014**, *2014*, 395637. [CrossRef] [PubMed]
24. Kalakwade, A.; Kavalapure, R.S.; Gharge, S.; Alegaon, S.G.; Ranade, S.D.; Wong, L.S.; Ramu, R. Heterocyclic compounds with diverse biological activities: A review of quinazoline and quinazolinone derivatives. *Results Chem.* **2026**, *19*, 102932. [CrossRef]
25. Barona-Gómez, F.; Wong, U.; Giannakopulos, A.E.; Derrick, P.J.; Challis, G.L. Identification of a Cluster of Genes that Directs Desferrioxamine Biosynthesis in Streptomyces coelicolor M145. *J. Am. Chem. Soc.* **2004**, *126*, 16282–16283. [CrossRef] [PubMed]
26. Yang, J.; Banas, V.S.; Patel, K.D.; Rivera, G.S.M.; Mydy, L.S.; Gulick, A.M.; Wencewicz, T.A. An acyl-adenylate mimic reveals the structural basis for substrate recognition by the iterative siderophore synthetase DesD. *J. Biol. Chem.* **2022**, *298*, 102166. [CrossRef] [PubMed]

27. Chen, X.-W.; Rao, L.; Chen, J.-L.; Zou, Y. Unexpected assembly machinery for 4(3H)-quinazolinone scaffold synthesis. *Nat. Commun.* **2022**, *13*, 6522. [CrossRef] [PubMed]
28. Ogasawara, Y.; Dairi, T. Biosynthesis of Oligopeptides Using ATP-Grasp Enzymes. *Chem. Eur. J.* **2017**, *23*, 10714–10724. [CrossRef] [PubMed]
29. Zeng, S.; Liu, J.; Anankanbil, S.; Chen, M.; Guo, Z.; Adams, J.P.; Snajdrova, R.; Li, Z. Amide Synthesis via Aminolysis of Ester or Acid with an Intracellular Lipase. *ACS Catal.* **2018**, *8*, 8856–8865. [CrossRef]
30. Kieser, T.; Bibb, M.J.; Chater, K.F.; Butter, M.; Hopwood, D.A.; Bittner, M.; Buttner, M.J. *Practical Streptomyces Genetics: A Laboratory Manual*; John Innes Foundation: Norfolk, UK, 2000.
31. Blin, K.; Shaw, S.; Vader, L.; Szenei, J.; Reitz, Z.L.; Augustijn, H.E.; Cediel-Becerra, J.D.D.; de Crécy-Lagard, V.; Koetsier, R.A.; Williams, S.E.; et al. antiSMASH 8.0: Extended gene cluster detection capabilities and analyses of chemistry, enzymology, and regulation. *Nucleic Acids Res.* **2025**, *53*, W32–W38. [CrossRef] [PubMed]
32. Schwyn, B.; Neilands, J.B. Universal chemical assay for the detection and determination of siderophores. *Anal. Biochem.* **1987**, *160*, 47–56. [CrossRef] [PubMed]

Disclaimer/Publisher's Note: The statements, opinions and data contained in all publications are solely those of the individual author(s) and contributor(s) and not of MDPI and/or the editor(s). MDPI and/or the editor(s) disclaim responsibility for any injury to people or property resulting from any ideas, methods, instructions or products referred to in the content.